Acta Geochim (2019) 38(2):173–189
https://doi.org/10.1007/s11631-018-00312-y

ORIGINAL ARTICLE

Is seawater geochemical composition recorded in marine carbonate? Evidence from iron and manganese contents in Late Devonian carbonate rocks

Zhe Wang[1] · Wen Guo[1,2] · Ting Nie[1] · Haoran Ma[1] · Tianzheng Huang[1] ·
Yuanlin Sun[1] · Bing Shen[1]

Received: 12 April 2018 / Revised: 25 July 2018 / Accepted: 26 December 2018 / Published online: 3 January 2019

Abstract Iron and manganese are the important redox-sensitive elements in the ocean. Previous studies have established a series of paleo-depositional redox proxies based on the form and content of iron in sedimentary rocks (e.g., degree of pyritization, Fe_{HR}/Fe_T, Fe/Al). These proxies were developed and applied on siliciclastic-rich marine sediments. Although marine carbonate rocks are generally considered to preserve the geochemical signals of ancient seawater, neither Fe nor Mn content in marine carbonate rocks (Fe_{carb}, Mn_{carb}) has been independently used as a proxy to quantify environmental cues in paleo-oceans. Both Fe and Mn are insoluble in oxic conditions (Fe_2O_3, $Fe(OH)_3$, MnO_2), while their reduced forms (Fe^{2+} and Mn^{2+}) are soluble. Therefore, oxic seawater should have low concentrations of dissolved Fe^{2+} and Mn^{2+}, and accordingly carbonate rocks precipitated from oxic seawater should have low Fe_{carb} and Mn_{carb}, and vice versa. To evaluate whether Fe_{carb} and Mn_{carb} can be used to quantify oxygen fugacity in seawater, we measured Fe_{carb} and Mn_{carb} of Upper Devonian marine carbonate rocks collected from nine sections in South China. Fe_{carb} of intraplatform basin samples was significantly higher than that of shelf samples, while shelf and basin samples had comparable Mn_{carb}. The modeling result indicates that the dramatic difference in Fe_{carb} cannot be explained by variation in oxygen fugacity between the shelf and basin seawater. Instead, both Fe_{carb} and Mn_{carb} appear to be more sensitive to benthic flux from sediment porewater that is enriched in Fe^{2+} and Mn^{2+}. Porewater Fe^{2+} and Mn^{2+} derive from bacterial iron and manganese reduction; flux was controlled by sedimentation rate and the depth of the Fe(Mn) reduction zone in sediments, the latter of which is determined by oxygen fugacity at the water–sediment interface. Thus, high Fe_{carb} of the basin samples might be attributed to low sedimentation rate and/or low oxygen fugacity at the seafloor. However, invariant Mn_{carb} of the shelf and basin samples might be the consequence of complete reduction of Mn in sediments. Our study indicates that marine carbonate rocks may not necessarily record seawater composition, particularly for benthic carbonate rocks. The influence of benthic flux might cause carbonate rocks' geochemical signals to deviate significantly from seawater values. Our study suggests that interpretation of geochemical data from carbonate rocks, including carbonate carbon isotopes, should consider the process of carbonate formation.

Keywords Carbonate rocks · Fe content · Mn content · Oxygen fugacity · Benthic flux

1 Introduction

It is widely accepted that the seawater geochemical composition can be faithfully recorded in marine carbonate rocks, if diagenetic alteration can be ruled out. As such, reconstruction of seawater geochemical composition and

Electronic supplementary material The online version of this article (https://doi.org/10.1007/s11631-018-00312-y) contains supplementary material, which is available to authorized users.

✉ Yuanlin Sun
ylsun@pku.edu.cn

✉ Bing Shen
bingshen@pku.edu.cn

[1] Key Laboratory of Orogenic Belts and Crustal Evolution, MOE, School of Earth and Space Sciences, Peking University, Beijing 100871, China

[2] Nanjing Institute of Geology and Paleontology, Chinese Academy of Science, Nanjing 210008, China

biogeochemical cycles in paleo-oceans have been approached with various geochemical proxies extracted from carbonate rocks (Frimmel 2009; Higgins and Schrag 2012; Kampschulte et al. 2001; Kampschulte and Strauss 2004; Knoll et al. 1986; Pogge von Strandmann et al. 2014; Webb and Kamber 2000; Zhao et al. 2009). For example, carbonate carbon isotopes ($\delta^{13}C_{carb}$) have been canonically interpreted as recording the isotopic composition of dissolved inorganic carbon (DIC) in seawater (Kump and Arthur 1999), and thus have been widely used in chemostratigraphic correlation (Halverson et al. 2005; Knoll et al. 1986; Zhu et al. 2007). In addition, trace amounts of sulfate incorporated into the carbonate crystal lattice (Pingitore et al. 1995), collectively known as carbonate associated sulfate (CAS), are believed to record the sulfur isotopic composition of seawater sulfate (Fike et al. 2015; Kampschulte et al. 2001; Kampschulte and Strauss 2004); such a proxy might be preserved in early diagenesis and dolomitization (Gill et al. 2008; Kah et al. 2004). Moreover, it is proposed that seawater Mg isotopic compositions (δ^{26}Mg) can be preserved in marine carbonate, although it is still debated which particular carbonate component is the most reliable archive (Higgins and Schrag 2012; Ma et al. 2017; Pogge von Strandmann et al. 2014). In addition to various stable isotope systems, marine carbonate rocks have been used to reconstruct seawater elemental and radiogenic isotopic compositions, including rare earth elements (REEs), and strontium and neodymium isotopes. Shale-normalized REE data extracted from marine carbonate rocks of different ages demonstrate a similar light REE (LREE) depleted pattern (Nothdurft et al. 2004; Webb and Kamber 2000), while Sr and Nd isotopic compositions of paleo-oceans are mostly derived from marine carbonate (Edmonds 1992; Jones and Jenkyns 2001; Richter et al. 1992; Shaw and Wasserburg 1985), although bioapatite (e.g. conodonts) has been used as well (e.g., Ruppel et al. 1996; Saltzman et al. 2014; Chen et al. 2018).

Because the geochemical composition of carbonate rocks can be altered during diagenesis, evaluations must be carefully assessed before data interpretation. In addition to petrographic observation, which provides the first-hand assessment, various geochemical proxies, including the Mn/Sr ratio (Kah et al. 2012), the absolute values of oxygen isotopes, and the correlation of carbon and oxygen isotopes (Banner and Hanson 1990; Jacobsen and Kaufman 1999; Knauth and Kennedy 2009), have been applied in diagenetic evaluation. For carbonate rocks that have passed through diagenetic evaluations, geochemical compositions have been interpreted to record seawater composition.

Using carbonates as an archive of seawater geochemical composition assumes that marine carbonates precipitated within seawater. However, most carbonates were actually precipitated at seafloor near the water–sediment interface (WSI) in non-pelagic settings. When precipitating at the seafloor, marine carbonate is affected by both seawater and sediment porewater. For example, significant benthic fluxes have been widely observed along the modern seafloor. Unlike oxic seawater, benthic fluxes are particularly enriched in Fe^{2+} and Mn^{2+}, generating porewater-seawater concentration gradients and allowing the diffusion from porewater to seawater (Severmann et al. 2010; John et al. 2012; Cai et al. 2014, 2015; Wehrmann et al. 2014). In addition, porewater DIC that derives from organic matter degradation can be delivered to the seafloor (Cai et al. 2015), contributing to benthic carbonate precipitation. Under the influence of benthic flux, the geochemical composition of benthic carbonate can vary from that of seawater. Accordingly, the potential impact of benthic flux on marine carbonate rocks needs further exploration.

In this study, we focused on Fe and Mn contents in carbonate rocks. Iron and manganese are both redox-sensitive elements. Ferric Fe(III) is rather insoluble in neutral to basic pH solution, and readily precipitates as iron oxides (hematite, Fe_2O_3) or iron oxyhydroxides ($Fe(OH)_3$). Bacterial reduction of ferric Fe in suboxic conditions generates ferrous Fe(II) that is soluble at all pH conditions (Nealson and Myers 1990). Similarly, manganese is dominated by Mn(IV) in the form of MnO_2 in oxic Earth surface, while Mn(II) mainly derived from anaerobic bacterial reduction of Mn(IV) is soluble (Myers and Nealson 1988). Therefore, both Fe(nM) and Mn(μM) have extremely low concentrations in oxic seawater (Bruland et al. 2014). In contrast, both Fe reduction and Mn reduction take place in suboxic-anoxic conditions (Canfield and Thamdrup 2009; Canfield et al. 1993), resulting in an accumulation of Mn^{2+} and Fe^{2+} in high concentrations in anoxic seawater/porewater. An Fe speciation method has been developed to reconstruct seawater redox conditions. Two proxies have been used in this methodology: Fe_{HR}/Fe_T (the ratio between highly reactive Fe and total Fe) and Fe_{py}/Fe_{HR} (the degree of pyritization or the ratio of pyrite Fe content with respect to highly reactive Fe) (Raiswell and Canfield 1998; Poulton and Raiswell 2002; Lyons and Severmann 2006; Poulton and Canfield 2011). The Fe speciation method was developed based on siliciclastic sediments; its implication for carbonate rocks has been proposed recently (Clarkson et al. 2014).

Cathodoluminescence (CL) is an efficient way to evaluate Mn and Fe contents in carbonate rocks (Barbin et al. 1991; Budd et al. 2000), and has been used in the evaluation of diagenetic history of carbonates (Pierson 1981). In CL microscopy, Mn is the stimulator while Fe is the quencher of luminescence (Budd et al. 2000; Machel 1985; Pierson 1981). Carbonate with low Mn and Fe concentrations is characterized by non-luminescence, indicating its deposition in oxic seawater, while carbonate precipitated in suboxic conditions has high Mn but low Fe contents, and displays bright luminescence. In contrast, carbonate formed in anoxic environments with both high Mn and Fe contents shows dull luminescence. CL is a powerful tool in determining the depositional environment of marine carbonates; however, this method can only provide a qualitative estimation of redox conditions or oxygen fugacity during carbonate formation.

Until now, neither Fe(II) or Mn(II) contents in carbonate (Fe_{carb} and Mn_{carb}) has been independently used as a proxy in paleoenvironment studies. As one of the four components of reactive Fe in the Fe speciation analysis (Anderson and Raiswell 2004; Poulton and Canfield 2005), Fe_{carb} alone has not been used in environmental interpretation. Even less is known about the meaning of Mn_{carb}, except that Mn/Sr ratio is used for diagenetic evaluation of carbonate (Jacobsen and Kaufman 1999; Kaufman and Knoll 1995). To explore whether Fe_{carb} and Mn_{carb} of marine carbonate can be used to constrain the redox condition of seawater, we measured Fe_{carb} and Mn_{carb} of Late Devonian marine carbonates from nine sections in South China. Then, a numerical model was developed to evaluate the applicability of Fe_{carb} in paleoenvironment study.

2 Geologic setting

Carbonate samples were collected from nine sections in South China (Fig. 1), including the following sections: the Daposhang of Changshun County (Guizhou); Dazhai, Madao, and Changtang of Dushan County (Guizhou); Xiada, Duli-A, and Duli-B of Nandan County (Guangxi), Baisha of Yangshuo County (Guangxi); and Panlong of Wuxuan County (Guangxi). Sampling intervals are bracketed between the Late Devonian (the Frasnian Stage and the Famennian Stage, 382.7–358.9 Ma) and the early Carboniferous (the Tournaisian Stage, 358.9–346.7 Ma), during South China was the site of development of numerous offshore carbonate platforms transected by multiple narrow intraplatform basins. Such paleogeographic configuration might be attributed to the N–NE migration of the South China Block since the Middle Devonian. Trans-tensional tectonic movement resulted in the gradual fragmentation of the southern part of the South China Block and the development of two major sets of trans-tensional rift basins in Guangxi Province (Chen et al. 2001a). One set of *en echlon* basins formed as a result of reactivation of antecedent NE-SW sinistral strike-slip faulting along the deep-seated basement zone, while the other set of rhomb-shaped basins might be related to movement of a sinistral strike-slip fault (Chen et al. 2001a, b, 2006). In the Late Devonian to Early Carboniferous, the Dazhai, Madao, and Panlong Sections were located on carbonate platforms, representing shallow marine depositions (Fig. 1). The platform succession is characterized by massive algal, oolitic, and shelly wackestone, packstone, and grainstone of the Rongxian Formation (Fig. 2a–d). The other six sections were deposited in successional intraplatform basin environments (Fig. 1) represented by the Gubi Formation (from Frasian to lower Famennian) and the Wuzhishan Formation (Famennian to lower Tournasian). The Wuzhishan Formation can be correlated with the Daihua (Famennian) and Wangyou (Tournasian) Formations in Guizhou Province. The Gubi Formation is composed of thin- to medium-bedded wackestone and laminated limestone (Chang et al. 2017), while the Wuzhishan Formation is characterized by thin-bedded and nodular lime mudstone and wackestone, with occasional packstone (Fig. 2e, f). Sampling intervals are plotted in Fig. 3. The detailed conodont biostratigraphic framework is reported in the Daposhang (Ji 1989), Dazhai, Duli-A, and Changtang (Nie et al. 2016), and Baisha Sections (Chang et al. 2017). A detailed description of studied sections is included in the supplementary information.

3 Methods

Fresh carbonate samples were split with a rock saw and mirrored thin and thick sections were prepared from each split. Sample powders were collected from thick sections using a hand-held micro-drill (with a drill bit 0.2 mm in diameter). The sampling was guided by petrographic observation of mirrored thin sections. Three carbonate components were recognized and sampled separately: micrite, calcispar, and biogenic clasts. Although clasts included fossil fragments of brachiopod, echinoderm, gastropod, ostracod, and foraminifera, only the brachiopod shells were large enough for sampling. For brachiopod coquinoid limestone samples (in the Changtang, Duli-A, and Dazhai Sections), sample powders were collected from polished rock slabs using a hand-held micro-drill.

The dissolution procedure followed the sequential extraction method of carbonate Fe developed by Poulton and Canfield (2005). A buffering solution consisting of a mixture of acetic acid and ammonium acetate was prepared, and pH 4.5 was precisely achieved by changing the mixing ratio of acetic acid and ammonium acetate. About 50 mg sample powder was carefully weighed in an electronic balance and dissolved in 10 ml buffering solution. Reaction was allowed in a shaking table at 50 °C for 48 h. After centrifugation, 0.5 ml supernatant was collected and dried in a hot plate. The insoluble fraction was re-dissolved in 2% nitric acid, ready for elemental composition analysis. This dissolution method can guarantee complete

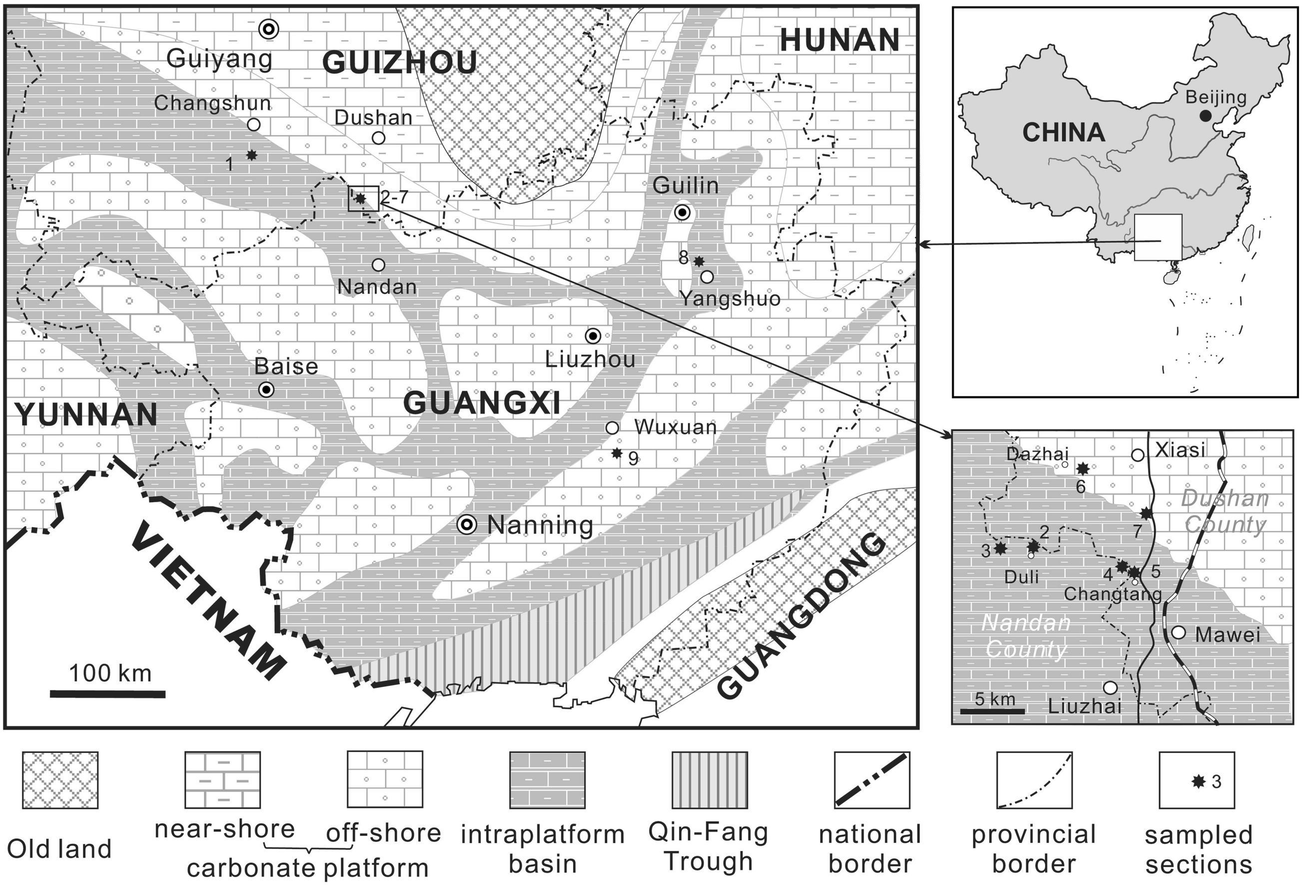

Fig. 1 Late Devonian paleogeographic map of the Yangtze Block, South China. Sample locations are marked by black dots. 1. Daposhang; 2. Duli-A; 3. Duli-B; 4. Xiada; 5. Changtang; 6. Dazhai; 7. Madao; 8. Baisha; and 9. Panlong

dissolution of carbonate minerals (aragonite, calcite, and dolomite), while oxides (Fe_2O_3, Fe_3O_4, and MnO_2) and sulfide (FeS_2) remain unaffected (Poulton and Canfield 2005).

The elemental compositions were determined by Spectra Blue Sop Inductively Coupled Plasma Optical Emission Spectrometry (ICP-OES) at Peking University. A series of gravimetric standard solutions with elemental concentrations ranging from 0.1 to 10 ppm were prepared. The calibration curve of each element was first established by measuring all the standard solutions before sample analyses. Analytical precision was better than 5% for all elements. In calculations, Ca and Mg were converted to carbonate minerals, i.e. $CaCO_3$ and $MgCO_3$, respectively, and the carbonate fraction was represented by the total mass of $CaCO_3$ and $MgCO_3$. The elemental compositions of other elements (Fe, Mn, Sr) were calculated based on carbonate fraction.

4 Results

Fe and Mn contents in the carbonate component (Fe_{carb} and Mn_{carb}) are listed in Table S1 and plotted in Fig. 4. Before further data analysis, this study considered the effect of carbonate rocks' Mg/Ca on Fe_{carb} and Mn_{carb}. The content of Mg_{carb} and Ca_{carb} is related to Mg^{2+} and Ca^{2+} in seawater. Aragonite and high-magnesium calcite (> 4 mol% $MgCO_3$) are preferentially precipitated from aragonite seawater (Mg/Ca > 2 mol/mol), while low-magnesium calcite precipitates from a calcite sea (Mg/Ca < mol/mol) (Hardie 1996; Stanley and Hardie 1998, 1999). The carbonate rocks returned abnormally high Fe_{carb} in the case of high-magnesium samples (> 4 mol% $MgCO_3$). This phenomenon is presumably due to the substitution of Mg^{2+} in the carbonate lattice for Ca^{2+}; lattice defects created by the smaller ionic radius of Mg^{2+} also cause Fe^{2+} to enter the carbonate lattice (Mazzullo 1992). Therefore, high-magnesium samples were excluded from our data analysis. The Fe_{carb} and Mn_{carb} results of the nine sections are summarized in Table 1.

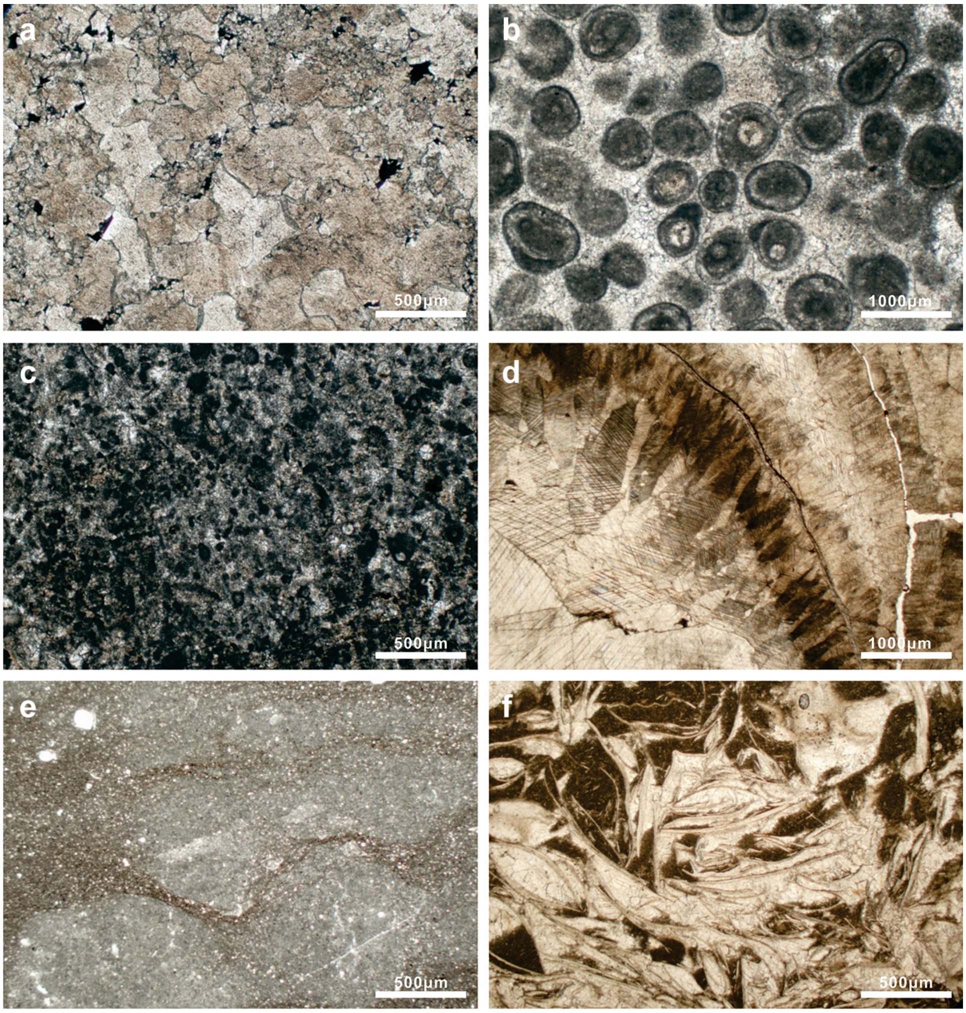

Fig. 2 Photomicrographs showing the texture of Late Devonian carbonate samples: **a** dolomitic limestone from the bottom part of Panlong Section; **b** oolitic packstone from the Dazhai Section; **c** peloid wackestone from the Panlong Section; **d** shelly packstone from the Dazhai Section, composed of densely packed shells of the rhynchonellid brachiopod *Dzieduszyckia*; **e** argillaceous limestone from the Changtang Section, showing distinguished lime-rich and mud-rich components; and **f** shelly wackestone from the Changtang Section, consisting of disarticulated shells of the rhynchonellid brachiopod *Dzieduszyckia*

5 Diagenetic evaluation

The geochemical composition of carbonate rocks can be altered during diagenesis. Therefore, potential diagenetic alteration should be evaluated before data interpretation.

Rock fabric tends to be altered during diagenesis, e.g. elimination of original fabric during recrystallization as well as non-mimic replacement in dolomitization (Banner et al. 1988). Thus, petrographic observation provides the most straightforward evidence for diagenetic alteration. The texture and fabric of all studied carbonate rocks was recognized. In this study, sample powders were collected by using a micro-mill (with bit size of 0.5 mm), warranting the millimetric spatial resolution in sampling. Sampling was component-based (i.e. differentiation of micrite, calcispar, and biogenic clasts), and was guided by petrographic observation in thin section. In this method, recrystallization regions and hydrothermal veins, if any, can be avoided during sampling.

CL has been widely applied in diagenetic evaluation of diagenesis. CL is controlled by the absolute concentrations of Mn and Fe in carbonate (Mn_{carb} and Fe_{carb}) and by the Mn_{carb}/Fe_{carb} ratio (Pierson 1981). In general, pristine marine carbonate (i.e. precipitated in oxic seawater) that is not significantly altered in diagenesis shows non-luminescence (i.e. low Mn and Fe contents), while diagenetically altered carbonate displays either bright luminescence (i.e. high Mn but low Fe content, reflecting early diagenesis in suboxic conditions) or dull luminescence (i.e. high Mn and high Fe, reflecting late diagenesis in anoxic conditions). The studied carbonate samples displayed non-luminescence to dull luminescence (Fig. 5). However, we suggest that diagenesis may not be the only interpretation of varying luminescence (see below).

Strontium and manganese contents in carbonate have been used in diagenesis as well (Kah et al. 2012; Gilleaudeau and Kah 2013) because Sr tends to be expelled from the carbonate lattice in early diagenesis, while Mn increases during burial. Based on principle, diagenetic

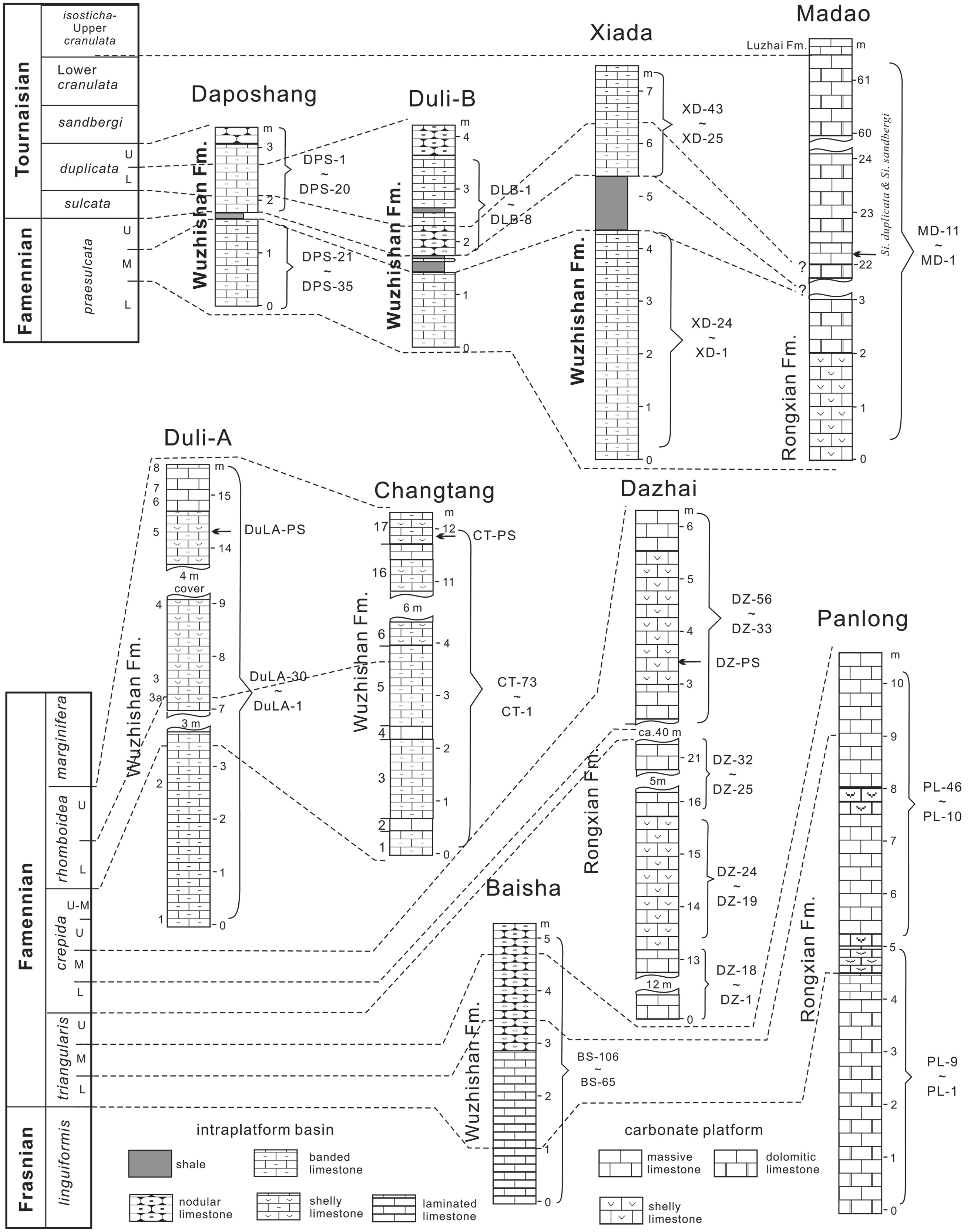
Tournaisian
isosticha-Upper cranulata
Lower cranulata
sandbergi
duplicata
U
L
sulcata
Famennian
praesulcata
U
M
L
Daposhang
Duli-B
Xiada
Madao
Luzhai Fm.
Wuzhishan Fm.
Rongxian Fm.
DPS-1 ~ DPS-20
DPS-21 ~ DPS-35
DLB-1 ~ DLB-8
XD-43 ~ XD-25
XD-24 ~ XD-1
MD-11 ~ MD-1
Si. duplicata & Si. sandbergi
Duli-A
Changtang
Dazhai
Panlong
Baisha
DuLA-PS
DuLA-30 ~ DuLA-1
4 m cover
3 m
6 m
CT-PS
CT-73 ~ CT-1
DZ-56 ~ DZ-33
DZ-PS
ca.40 m
DZ-32 ~ DZ-25
5m
DZ-24 ~ DZ-19
DZ-18 ~ DZ-1
12 m
PL-46 ~ PL-10
PL-9 ~ PL-1
BS-106 ~ BS-65
Frasnian
linguiformis
triangularis
crepida
rhomboidea
marginifera
U-M
intraplatform basin
shale
banded limestone
nodular limestone
shelly limestone
laminated limestone
carbonate platform
massive limestone
dolomitic limestone
shelly limestone
m

◀**Fig. 3** Conodont biostratigraphic correlation among the studied sections. The conodont zonation for the Duli-A, Changtang, and Dazhai Sections is adopted from Nie et al. (2016), for the Baisha Section from Chang et al. (2017), and for the Daposhang Section from Ji (1989); the *Siphonodella sulcata* Zone is amended based on unpublished data. Other sections are based on unpublished data

evaluation has been approached with Mn/Sr ratios. It is proposed that carbonates with low Mn/Sr ratios (< 10) can be regarded as least altered, suggesting potential preservation of the stratigraphic trend of geochemical signals (e.g. carbonate carbon isotopes) and applicability in chemostratigraphic correlation. In contrast, samples with high Mn/Sr may indicate possible alteration of stratigraphic trends (Kaufman and Knoll 1995). Mn/Sr ratios of the analyzed carbonate samples were low, 0.024 (2.5% quantile value) to 4.113 (97.5% quantile) (Table S1), arguing against diagenetic alteration of our samples.

Although petrographic observation, CL and Mn/Sr ratios indicate that the studied carbonate samples have not been significantly altered by diagenesis, some of these canonical interpretations may not be valid if carbonate was precipitated near WSI.

6 Discussion

6.1 Fe_{carb} and Mn_{carb} variation of different carbonate components

Three carbonate components were recognized in the studied samples: micrite, calcspar, and biogenic clasts (Figs. 3, S1, S2, S3). There are three possible sources of micrite in the modern ocean: disintegration of weakly calcified green algae, such as *Helimeda* and *Penicillus* (Wefer 1980), breakage of biogenic carbonate grains (micritization) (James and Choquette 1983), and inorganic or microbial-induced precipitation from seawater or within marine porewater (Munnecke and Samtleben 1996). Among the three possible sources, calcified green algae represent the most important micrite producer in the modern ocean, but it is unclear whether the algae that can generate micrite had evolved or become ecologically important by the late Paleozoic (Kaźmierczak et al. 1996; Riding 1991;

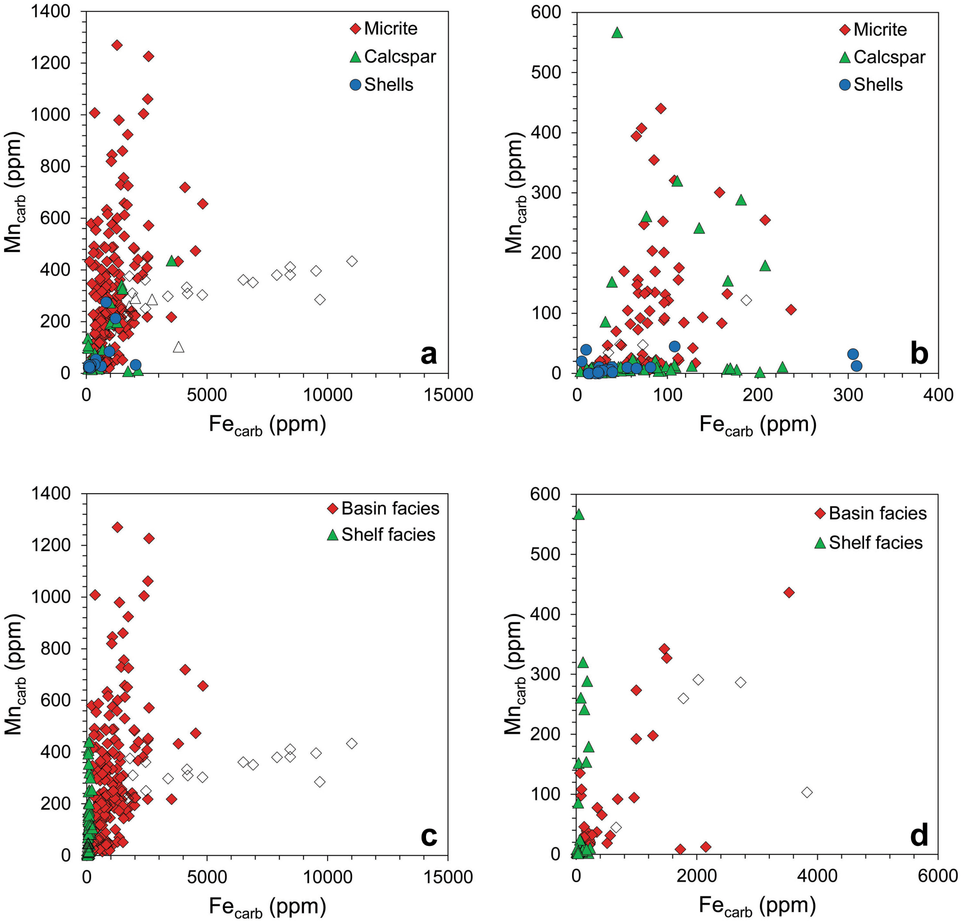

Fig. 4 Fe_{carb} versus Mn_{carb} cross-plots. Open symbols represent partially dolomitized samples with Mg/Ca (mol/mol) > 4%, while solid symbols represent various carbonate components (**a**, **b**) or different depositional environment (**c**, **d**). **a** Samples from basin sections; **b** samples from shelf sections; **c** micrite samples from different sedimentary facies; and **d** calcspar samples from different sedimentary facies

Table 1 Summarized measurement of the Fe, Mn contents in carbonate component (Fe_{carb}, Mn_{carb}) from the nine studied sections

Section and facies type	Sampled interval and formation	Component	Number	Fe_{carb} (ppm)		Mn_{carb} (ppm)	
				Range	Mean	Range	Mean
Madao, carbonate platform	D/C boundary, Rongxian Fm	Micrite	8	25.5–128.2	56.7	20.9–82.3	45.2
Duli-B, intraplatform basin	D/C boundary, Wuzhishan Fm	Micrite	8	284.4–2529.7	1437.5	54.6–846.0	268.8
Xiada, intraplatform basin	D/C boundary, Wuzhishan Fm	Micrite	43	231.1–4820.0	1068.3	49.6–1270.0	386.5
Daposhang, intraplatform basin	D/C boundary, Wuzhishan Fm	Micrite	35	305.9–1726.7	909.6	95.9–820.0	308.7
Dazhai, carbonate platform	lower Famennian, Rongxian Fm	Micrite	34	9.2–131.0	60.2	2.0–31.7	12.6
		Calcispar	64	3.6–227.2	57.0	1.7–24.3	7.7
		Brachiopod shell	21	5.0–309.2	60.5	0.0–45.0	10.7
Duli-A, intraplatform basin	Lower Famennian, Wuzhishan Fm	Micrite	34	134.1–1502.2	539.2	15.8–330.5	51.9
		Calcispar	19	61.4–2146.7	389.0	8.2–135.5	41.2
		Brachiopod shell	10	99.2–2043.7	373.2	19.8–53.8	29.1
Changtang, intraplatform basin	Lower Famennian, Wuzhishan Fm	Micrite	46	258.4–3525.	1180.5	38.4–490.0	188.0
		Calcispar	12	108.8–3528.9	1052.1	24.6–436.6	175.7
		Brachiopod shell	7	190.3–1211.6	609.4	25.4–275.4	99.8
Panlong, carbonate platform	F/F boundary, Rongxian Fm	Micrite	36	43.2–236.7	99.3	70.0–440.4	177.7
		Calcispar	9	31.3–208.1	110.4	86.1–567.2	250.1
*Baisha, intraplatform basin	F/F boundary, Gubi and Wuzhishan fms	Micrite	37	134.3–4527.4	1254.3	148.8–1061.6	489.0

*Cited from Chang et al. (2017)

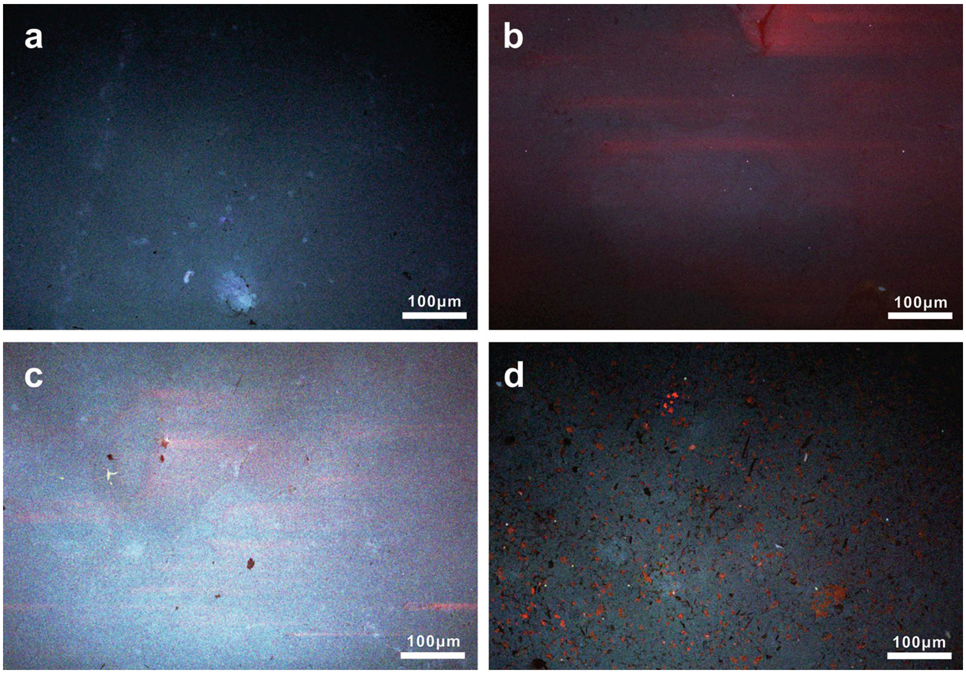

Fig. 5 Cathodoluminescence photomicrographs of Late Devonian carbonate samples: **a** non-luminescence of oolitic packstone from Dazhai Section (DZ-19); **b** non-luminescence of peloid wackestone from Panlong Section (PL-3), with calcispar showing dull luminescence; **c** non-luminescence of shelly packstone from coquinoid limestone (upper part of Dazhai Section, DZ-PS-23); and **d** non-luminescence of lime mudstone from the upper part of Daposhang Section (DPS-4), with calcispar showing dull luminescence

Verbruggen et al. 2005). On the other hand, inorganic precipitation of calcispar from normal seawater may not have been favored in the Phanerozoic because of the low carbonate saturation state (Dupraz et al. 2009; Mackenzie and Morse 1992). In most cases, precipitation of calcispar occurs during cementation that fills in the pore space between carbonate and/or siliciclastic grains (James and Choquette 1983). Cementation takes place when carbonate saturation is locally elevated, probably due to decomposition of organic matter that elevates pH and alkalinity (Gallagher et al. 2014). Calcispar could derive from diagenetic recrystallization, in which micrite and microcrystalline calcite/aragonite are dissolved followed by reprecipitation of coarser grained carbonate (James and Choquette 1983). Calcispar derived from recrystallization is normally characterized by a limpid rim and a turbid core. The biogenic carbonate grains in the samples were dominated by brachiopod shells composed of low-Mg calcite (Ma et al. 2017); other skeletons such as echinoderms, foraminifera, and ostracods were less common (Figs. 3, S1, S2, S3).

As compared with micrite and calcispar, brachiopod shells returned the lowest Mn_{carb} and Fe_{carb} contents, ranging from 0.0 (i.e. below the detection limit) to 275.4 ppm (mean = 32.0 ppm, n = 38) and 5.0–2043.7 ppm (mean = 243.9 ppm, n = 38), respectively. For shelf samples with lower Fe contents (< 100 ppm), micrite had higher Mn (mean = 82.2 ppm) than calcispar (mean = 25.0 ppm), whereas high Fe samples (> 100 ppm) had overlapping ranges of Mn_{carb} (Figs. 6, 7). For carbonate samples from basin sections, micrite and calcispar had overlapping ranges of Fe_{carb} but micrite had higher Mn_{carb} than calcispar (286.1 ppm vs. 93.3 ppm, Figs. 6, 7).

6.2 Fe_{carb} and Mn_{carb} variations in different depositional environments

Except for two outliers, micrite of shelf samples had lower Fe_{carb} than basin samples, while micrite of the shelf and basin samples had comparable Mn_{carb} (Figs. 6, 7). There was a crude positive correlation between Fe_{carb} and Mn_{carb} for basin samples. Shelf samples with low Fe content (< 200 ppm) had abnormally high Mn_{carb}, while Mn content remained low (< 100 ppm) when Fe_{carb} ranged from 200 to ~ 1000 ppm. At Fe_{carb} of 1000 ppm, Mn_{carb} returned a higher level, but seldom exceeded 400 ppm (Fig. 5). Samples with high Mn but low Fe contents were sourced from the Panlong Section (with sampling interval transecting the Frasnian-Famennian boundary). The cause of exceptionally high Mn content of the Panlong samples is unclear. We speculate that Mn enrichment in the Panlong might be related to the metallogenesis of the Xialei Mn ores in nearby regions (Zeng and Liu 1999).

6.3 Can Fe_{carb} indicate seawater redox condition?

It is widely accepted that elemental and isotopic compositions of marine carbonate may record the geochemical signature of seawater if diagenetic alteration can be confidently excluded (Banner 2004; Pelechaty et al. 1996) Thus, carbonate has often been used in paleoenvironment studies. For example, carbonate carbon isotopes ($\delta^{13}C_{carb}$) have long been used to indicate isotopic composition of DIC in seawater, and the stratigraphic variation of $\delta^{13}C_{carb}$ has been used for chemostratigraphic correlations at regional and global scales (Kaufman and Knoll 1995). Since Fe is a redox-sensitive element and Fe content in seawater ($[Fe]_{sw}$) is controlled by seawater oxygen fugacity, we explored whether Fe_{carb} can be used to record the redox condition of paleo-oceans.

In oxic conditions, Fe is dominated by Fe(III), which is rather insoluble at neutral to basic pH conditions. Fe(III) can be anaerobically reduced to soluble Fe(II) (Nealson and Myers 1990). Furthermore, because ferrous iron (Fe^{2+}) has a similar charge but smaller ionic radius compared to Ca^{2+}, Fe^{2+} readily substitutes for Ca^{2+} in the carbonate crystal lattice. The degree of substitution is determined by the concentration of Fe^{2+} in solution and the partitioning coefficient between carbonate and solution, the latter of which is affected by other factors, such as temperature (Morse and Bender 1990).

The amount of Fe^{2+} in seawater is determined by oxygen fugacity ($f(O_2)$). The chemical equation for ferrous iron oxidation by oxygen can be expressed as:

$$4Fe^{2+} + O_2 + 10H_2O = 4Fe(OH)_3\downarrow + 8H^+ \tag{1}$$

Because Fe_2O_3 and $Fe(OH)_3$ are insoluble, the equilibrium for Eq. 1 can be expressed as:

$$K = \frac{[H^+]^8}{[Fe^{2+}]^4 \times [O_2]} \tag{2}$$

where K is the equilibrium constant and $[H^+]$, $[Fe^{2+}]$, and $[O_2]$ are dissolved proton, ferrous Fe, and O_2 concentrations in seawater, respectively. Rearranging Eq. 2, we get:

$$\left[Fe^{2+}\right] = \left(\frac{[H^+]^8}{K \times [O_2]}\right)^{1/4} \tag{3}$$

Dividing Eq. 3 by $[Ca^{2+}]$ on both sides, we get:

$$\left(\frac{Fe^{2+}}{Ca^{2+}}\right) = \frac{1}{\left[Ca^{2+}\right]}\left(\frac{[H^+]^8}{K \times [O_2]}\right)^{1/4} \tag{4}$$

$\left(\frac{Fe^{2+}}{Ca^{2+}}\right)$ is the Fe/Ca molar ratio in seawater. The amount of Fe in carbonate ($(Fe/Ca)_{carb}$) can be calculated by:

$$\left(\frac{Fe}{Ca}\right)_{carb} = \frac{D}{\left[Ca^{2+}\right]}\left(\frac{[H^+]^8}{K \times [O_2]}\right)^{1/4} \tag{5}$$

where *D* is the ratio of partitioning coefficients between Fe and Ca, i.e. $D = D_{Fe}/D_{Ca}$, during carbonate precipitation.

Fig. 6 Histograms of Fe_{carb} and Mn_{carb} from different depositional environments: **a** Fe_{carb} of micrite; **b** Mn_{carb} of micrite; **c** Fe_{carb} of calcispar; and **d** Mn_{carb} of calcispar

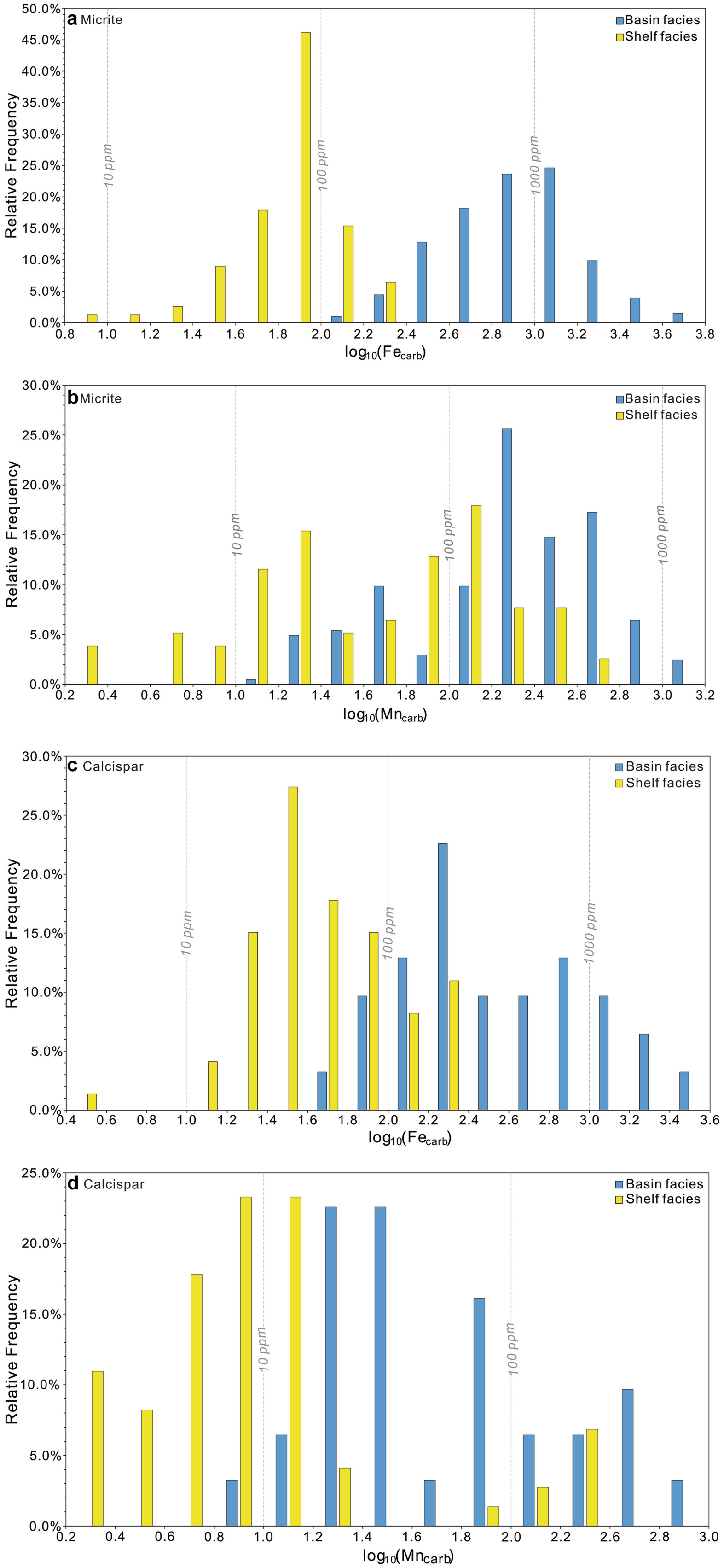

Fig. 7 Box-plots showing Fe_{carb} and Mn_{carb} of the Late Devonian carbonate samples. Box brackets delineate 25 and 75 percentiles, while the bar in the middle of the box represents the median of the values. Whiskers indicate 2.5 and 97.5 percentiles, and hollow dots are outliers. **a** Fe_{carb} of micrite; **b** Mn_{carb} of micrite; **c** Fe_{carb} of calcispar; and **d** Mn_{carb} of calcispar from different sections

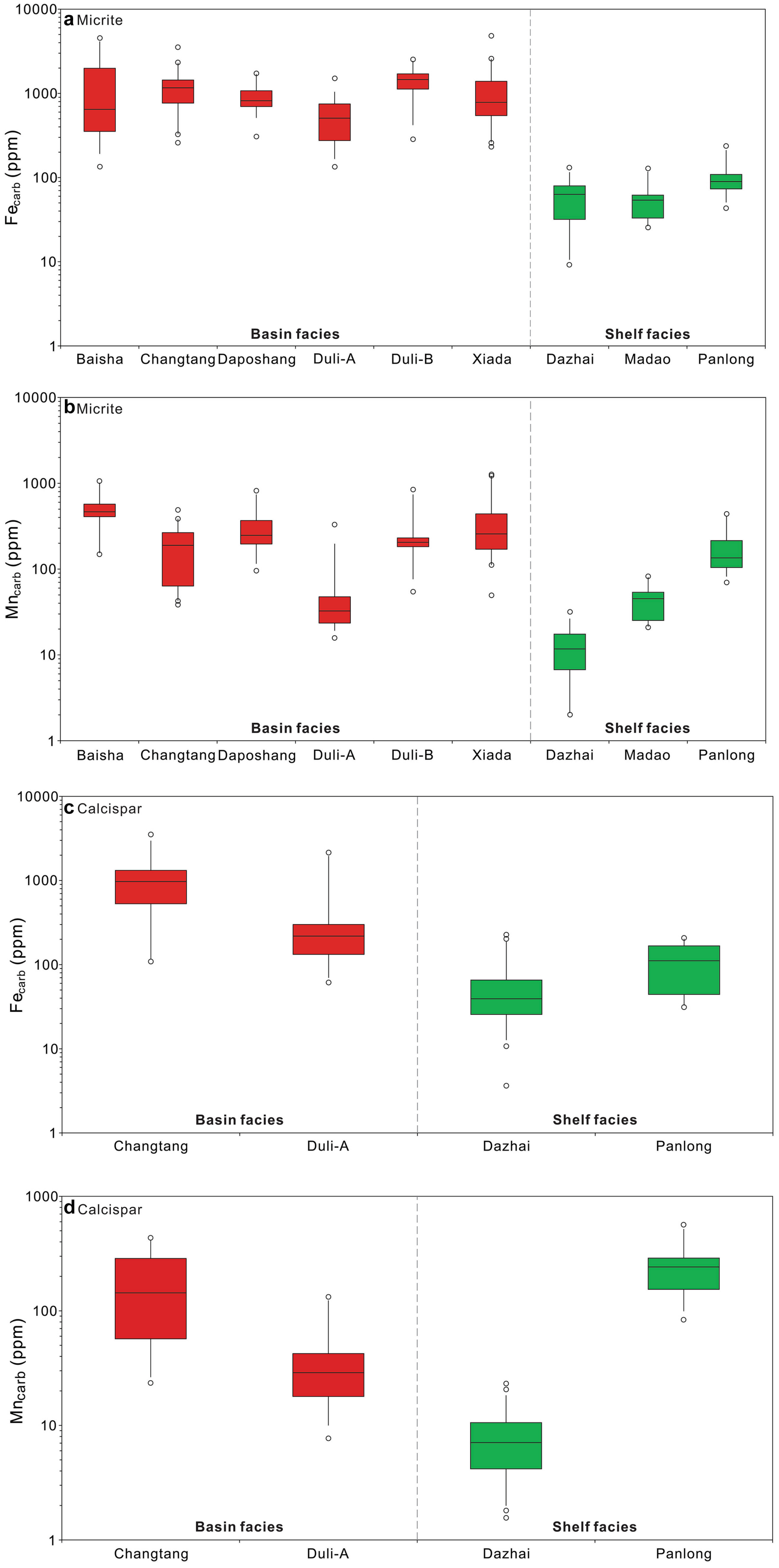

Equation 5 indicates that Fe content in carbonate is inversely correlated with the fourth root of O_2 concentration, suggesting that carbonate would have higher Fe_{carb} when precipitating from anoxic seawater (low oxygen fugacity), and vice versa.

Furthermore, if seawater and atmosphere are in equilibrium, the relationship between Fe_{carb} and atmospheric pO_2 level can be expressed by using Henry's law, $[O_2] = H^*pO_2$:

$$\left(\frac{\mathrm{Fe}}{\mathrm{Ca}}\right)_{carb} = \frac{\mathrm{D}}{[\mathrm{Ca}^{2+}]}\left(\frac{[\mathrm{H}^+]^8}{\mathrm{K} \times \mathrm{H} \times pO_2}\right)^{1/4} \tag{6}$$

By using Eq. 6, atmospheric pO_2 can be theoretically reconstructed from Fe_{carb} if seawater and atmosphere are in equilibrium. However, because the partitioning coefficients are loosely constrained, atmospheric pO_2 cannot be precisely calculated. We compared the shelf and basin carbonate samples by assuming, (1) shelf and basin seawater have similar $[Ca^{2+}]$ and pH, and (2) seawater in the shelf environment is in equilibrium with atmospheric pO_2. The oxygen fugacity in the basin environment can be calculated by the following:

$$[\mathrm{O}_2]_{basin} = \left(\frac{\left(\frac{\mathrm{Fe}}{\mathrm{Ca}}\right)^{shelf}_{carb}}{\left(\frac{\mathrm{Fe}}{\mathrm{Ca}}\right)^{basin}_{carb}}\right)^4 \times H \times pO_2 \tag{7}$$

where superscripts *shelf* and *basin* indicate the shelf and basin samples, respectively, and $[O_2]_{basin}$ refers to dissolved oxygen concentration in the basin environment. By assuming the atmospheric pO_2 level in the Late Devonian was equal to that of present day (0.21 atm) and seawater temperature of 25 °C (Sperling et al. 2015), Henry's constant for O_2 is set to 1.3 mmol/L/atm. The average values of Fe_{carb} for the shelf and basin samples were 77.9 and 1026.2 ppm, respectively. The estimated $[O_2]_{basin}$ was 0.009 μM or 0.286 μg/L (Fig. 8). This value is three orders of magnitude lower than the threshold for anoxic ($[O_2] < 200$ μg/L) (Libes 2009), suggesting that the basin environment was extremely anoxic and bacteria sulfate reduction occurred. This calculation represents the maximum estimation of $[O_2]_{basin}$ by assuming shelf seawater was in equilibrium with atmospheric pO_2. In fact, the shelf seawater could be less oxic, if oxygen consumption by organic matter degradation were considered.

The estimated $[O_2]_{basin}$ level based on Fe_{carb} contradicts paleontological evidence. The presence of benthic animal fossils, such as gastropods, ostracods, and echinoderms, strongly argues against extreme anoxic conditions in the basin sections (Figs. 3, S1, S2, S3). Therefore, seawater oxygen fugacity may not be the only control of Fe_{carb}, suggesting that the application of Fe_{carb} in paleoenvironment study is not straightforward. Below, we explore the controlling factors of Fe_{carb}.

6.4 Controls on Fe_{carb} and Mn_{carb}

Equation 6 indicates that Fe_{carb} and Mn_{carb} are controlled by the oxygen fugacity of seawater. However, our calculations indicate that the estimated $[O_2]_{basin}$ is too low and contradicts paleontological data (Figs. 3, S1, S2, S3). Although potential diagenetic alteration cannot be completely ruled out by petrographic observation, CL, and Mn/Sr ratios, diagenesis alone cannot explain systematically higher Fe_{carb} in basin sections. In fact, the above estimation assumes that seawater dissolved $[Fe^{2+}]$ is the only Fe source for carbonate, which might be true only when all carbonate precipitated from the water column. In fact, it is well known that Paleozoic marine carbonates were mainly produced by benthic carbonate-secreting organisms (Bartley and Kah 2004; Mackenzie et al. 2004; Mackenzie and Morse 1992; Tucker and Wright 1990), such as brachiopods, echinoderms, mollusks, corals, and bryozoans (Sepkoski and Miller 1985). Although modern foraminifera represent one of the most important carbonate producers in the ocean, and exhibit both benthic and planktonic lifestyle (Gupta 1999), Paleozoic foraminifera were exclusively benthic (falFrerichs 1971; Vachard et al. 2010). Benthic carbonate produced at or near SWI would be affected by both seawater and sediment porewater.

In the modern open ocean seafloor with relatively high oxygen fugacity, seawater is characterized by low $[Fe^{2+}]$. In contrast, sediment porewater is more reduced due to the consumption of dissolved O_2 by aerobic organic matter degradation. After complete depletion of O_2, organic matter undergoes anaerobic degradation by using oxides (e.g. MnO_2 and Fe_2O_3) or oxy-anions (e.g. nitrate and sulfate) as electron acceptors (Canfield and Thamdrup 2009; Canfield et al. 1993). Bacterial manganese and iron reduction can be expressed as:

$$\mathrm{CH_2O} + 2\mathrm{MnO_2} + \mathrm{H_2O} = \mathrm{HCO_3^-} + 2\mathrm{Mn^{2+}} + 3\mathrm{OH^-} \tag{8}$$

$$\mathrm{CH_2O} + 2\mathrm{Fe_2O_3} + 3\mathrm{H_2O} = \mathrm{HCO_3^-} + 4\mathrm{Fe^{2+}} + 7\mathrm{OH^-} \tag{9}$$

These reactions generate Fe^{2+}, Mn^{2+}, and HCO_3^- that derives from remineralization of organic matter, resulting in high concentrations of Fe^{2+} and Mn^{2+} in sediment porewater. As such, Fe^{2+} and Mn^{2+} concentration gradients are generated between porewater and seawater. The upward diffusion of porewater Fe^{2+} and Mn^{2+} into seawater generates benthic fluxes (Cai et al. 2014, 2015; John et al. 2012; Severmann et al. 2010; Wehrmann et al. 2014). When carbonate precipitates at the seafloor, benthic fluxes

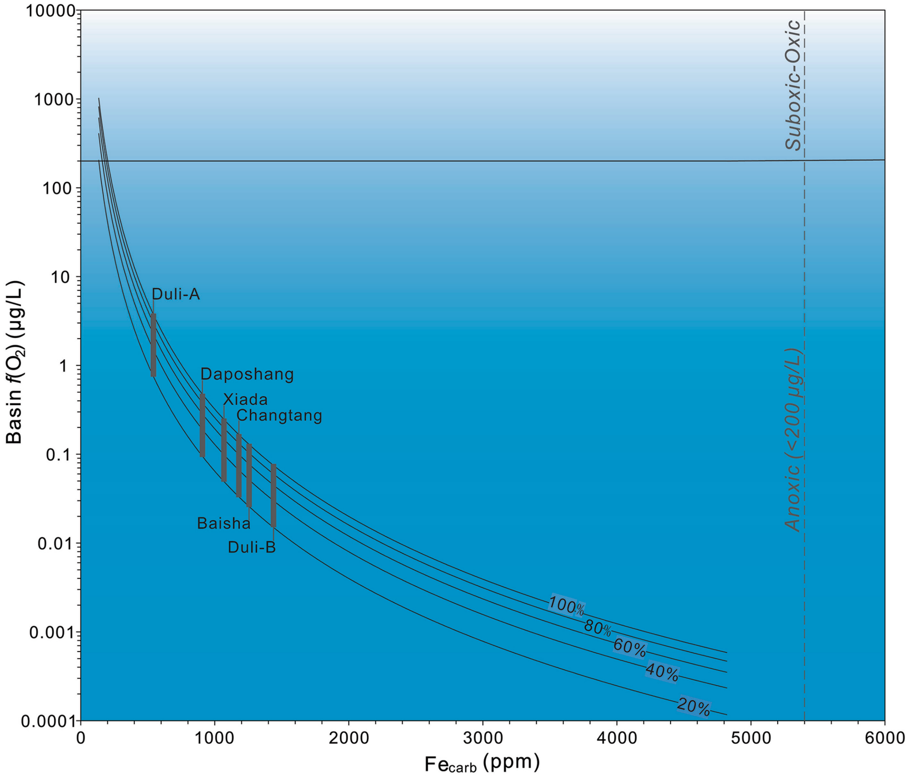

Fig. 8 Modeling results showing the relationship between Fe_{carb} and oxygen fugacity of seawater in the basin environment. Contour lines represent different oxygen fugacity in the shelf facies. 100% refers to the equilibrium between seawater and atmosphere; $[O_2]$ can be calculated by Henry's Law

of Fe^{2+} and Mn^{2+} can be incorporated into carbonate rocks, resulting in an increase of both Fe_{carb} and Mn_{carb}.

The Fe^{2+} and Mn^{2+} fluxes from sediment pore water are determined by concentration gradients between porewater and seawater, which can be expressed by:

$$\nabla_{Mn} = \frac{\left([Mn]_{pw} - [Mn]_{sw}\right)}{l_{Mn}} \tag{10}$$

$$\nabla_{Fe} = \frac{\left([Fe]_{pw} - [Fe]_{sw}\right)}{l_{Fe}} \tag{11}$$

where ∇_i is the one-dimensional concentration gradient of species i (Mn^{2+} and Fe^{2+}), and l_i is the depth of the Fe/Mn reduction zone below WSI. Subscripts *pw* and *sw* represent porewater and seawater, respectively. Because both $[Mn]_{sw}$ and $[Fe]_{sw}$ in oxic seawater are low (μM and nM level, respectively), the concentration gradient is mainly controlled by $[Mn]_{pw}$ and $[Fe]_{pw}$. High $[Mn]_{pw}$ and $[Fe]_{pw}$ require availability of organic matter and reactive Mn (i.e. MnO_2) and Fe (i.e. Fe_2O_3) in sediments. With the consideration of benthic fluxes, Mn and Fe concentration in benthic carbonate can be calculated by:

$$Fe_{carb} = \frac{\left([Fe]_{sw} \times K_{Fe} + \Delta_{Fe} \times D_{Fe}\right)}{A \times s \times \rho} \times M_{Fe} \tag{12}$$

where K_{Fe} is the partitioning coefficient of Fe between solution and carbonate, D_{Fe} the coefficient of diffusivity of Fe^{2+}, A area, s sedimentation rate, ρ the density of carbonate, and M_{Fe} the molecular weight of Fe (56 g/cm^3).

By ignoring $[Fe]_{sw}$ in oxic seawater and combining Eqs. 11 and 12, we arrive at:

$$Fe_{carb} = \frac{\left([Fe]_{pw} \times D_{Fe}\right)}{A \times s \times \rho \times l_{Fe}} \times M_{Fe} \tag{13}$$

Equation 13 indicates that Fe_{carb} is controlled by the following three parameters: $[Fe]_{pw}$, l_{Fe}, and s. Obviously, high Fe_{carb} is favored at low sedimentation rates, small l_{Fe} (i.e. shallow depth of iron reduction zone), and higher concentration of $[Fe]_{pw}$. If we compare the shelf and basin sections investigated in this study, the shelf sections have significantly higher sedimentation rate, as indicated by larger stratigraphic thickness (within the same conodont zone) (Fig. 2). Low sedimentation rate is accompanied by accumulated organic matter in sediment, enhancing O_2 consumption and shoaling the iron reduction zone (i.e. lower l_{Fe}). Therefore, high Fe_{carb} of the basin samples might be directly attributed to low sedimentation, which in turn leads to high flux of Fe^{2+} from sediment porewater.

Unlike Fe_{carb} that showed orders of magnitude difference between shelf and basin samples, the shelf and basin samples had an overlapping range of Mn_{carb}. This might be attributed to (1) Mn reduction before Fe reduction in sediments (Canfield et al. 1993), and (2) Mn content in upper continental crust is about 50 times less than Fe (775 vs. 39,200 ppm) (Rudnick and Gao 2003).

6.5 Does carbonate record seawater composition?

Our study indicates that Fe_{carb} and Mn_{carb} of Late Paleozoic carbonate are strongly affected by benthic fluxes from sediment porewater, suggesting that benthic carbonate does not necessarily record seawater geochemical composition. Therefore, the interpretation of geochemical data extracted from carbonate samples should consider the processes of carbonate formation. We suggest that only carbonate precipitated within the water column records seawater composition; benthic carbonate precipitated at the seafloor is suspected to be influenced by benthic flux from sediment porewater. Benthic carbonate is least likely to record seawater composition when the sedimentation rate and seafloor oxygen fugacity are low, whereas shallow marine carbonate formed in well-ventilated seawater, where benthic flux is low, is more likely to preserve seawater composition.

Carbonate carbon isotope ($\delta^{13}C_{carb}$) is the most widely used proxy in chemostratigraphic correlation (Kaufman et al. 1993; Knoll et al. 1986; Zhu et al. 2013). A $\delta^{13}C_{carb}$ gradient along the shallow-to-deep transect is commonly observed in sedimentary basins. Normally, shallow-water carbonate has higher $\delta^{13}C_{carb}$ values than deep-water carbonate. Traditionally, this gradient has been interpreted in terms of bathymetric isotopic gradients in seawater (Jiang et al. 2007; Lang et al. 2016; Shen et al. 2011).

Alternatively, our study suggests that the $\delta^{13}C_{carb}$ gradient could be generated by variation of sedimentation rate between shallow- and deep-water sections. Deposition of ^{12}C-enriched carbonate in the deep water environment might be attributed to a larger benthic flux that delivers ^{12}C-enriched DIC from porewater (Cai et al. 2014, 2015; Emerson et al. 2003). Large benthic flux is favored by low sedimentation rate (Eq. 13, Fig. 9). In addition, seafloor might have lower oxygen fugacity if the water depth is greater than the thickness of the surface mixing zone. Therefore, interpretation of $\delta^{13}C_{carb}$ data should also consider the processes of carbonate formation. Sedimentological analyses and petrographic observations are highly recommended to differentiate whether carbonate was precipitated in the water column or at the seafloor (i.e. benthic carbonate). In addition, an estimate of sedimentation rate based on high resolution biostratigraphic and chronostratigraphic framework would also provide additional constraints on data interpretation.

With the consideration of benthic flux in carbonate precipitation, there is no longer a clear cutoff between sedimentation and diagenesis. Sedimentary carbonate could also record signals of diagenesis, given that benthic flux delivers porewater material into seawater. Therefore, some traditional approaches or geochemical proxies in diagenetic evaluation warrant reconsideration. For example, bright or dull luminescence in CL imaging may not necessarily indicate a diagenetic origin of carbonate. Benthic carbonate with significant input from benthic flux would display similar luminescence. The Mn/Sr ratio should not be used either, because only Sr loss occurs in sediment, while Mn could be gained during benthic carbonate precipitation. Therefore, diagenetic alteration might be overestimated; some data might be explained by the influence of benthic flux.

Finally, we recommend using Fe_{carb} and Mn_{carb} as proxies to evaluate the potential influence of benthic flux. Samples with high Fe_{carb} and Mn_{carb} may indicate strong benthic flux, and accordingly are less likely to record seawater composition. Only carbonate samples with low Fe_{carb} and Mn_{carb} might be suitable for the reconstruction of seawater geochemical composition.

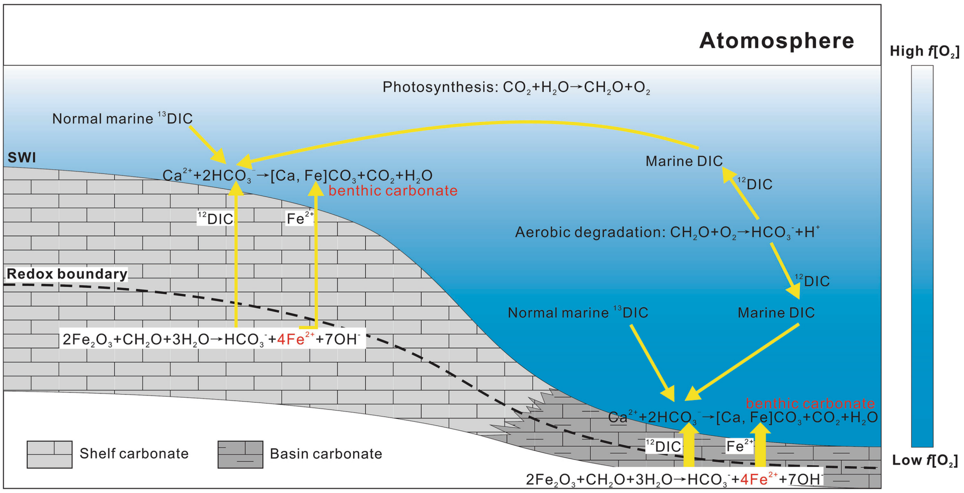

Fig. 9 Schematic diagrams showing how Fe_{carb} and Mn_{carb} are controlled by benthic fluxes from sediment porewater. Both values are affected by sedimentation rate and the depths of redox boundaries below which iron (manganese) reduction would occur. The thickness of arrows represents the intensity of Fe^{2+} and Mn^{2+} benthic fluxes

7 Conclusions

We measured Fe_{carb} and Mn_{carb} of Late Devonian carbonate samples from nine sections in South China. As compared with shelf carbonate samples, samples from basin sections had significantly higher Fe contents but comparable Mn contents. Modeling indicates that if seawater in the shelf environment was in equilibrium with atmospheric pO_2, basin seawater would be extremely anoxic with dissolved oxygen content < 1 μM, which is inconsistent with abundant benthic fossils, suggesting that seawater oxygen fugacity may not be the only control on Fe_{carb}. We suggest Fe_{carb} and Mn_{carb} might also be affected by benthic flux, bringing Fe^{2+} and Mn^{2+} from anoxic sediment porewater. High Fe_{carb} in deep-water carbonate might have resulted from a relatively low sedimentation rate as well as the shallow depth of the iron reduction zone in sediments. In contrast, the shelf and basin samples displaying comparable Mn_{carb} might be attributed to nearly complete reduction of Mn in sediments, given the low Mn content in the upper continental crust. Our study indicates that marine carbonate may not necessarily record seawater geochemical composition. Carbonate precipitated on the seafloor, i.e. benthic carbonate, would also be affected by benthic flux from sediment porewater. Therefore, interpretation of carbonate geochemical data should also consider the process of carbonate formation.

Acknowledgements This study was supported by National Science Foundation of China (Nos. 41172001 and 41772015 to Sun and No. 41772359 to Shen). We thank Prof. Linda Kah and one anonymous reviewer for constructive comments and suggestions.

References

Anderson TF, Raiswell R (2004) Sources and mechanisms for the enrichment of highly reactive iron in euxinic Black Sea sediments. Am J Sci 304:203–233

Banner JL (2004) Radiogenic isotopes: systematics and applications to earth surface processes and chemical stratigraphy. Earth Sci Rev 65(3–4):141–194

Banner JL, Hanson GN (1990) Calculation of simultaneous isotopic and trace element variations during water-rock interaction with applications to carbonate diagenesis. Geochimica et Cosmochimica Acta 54:3123–3137

Banner JL, Hanson GN, Meyers WJ (1988) Waterrock interaction history of regionally extensive dolomites of the Burlington-Keokuk formation (Mississippian): isotopic evidence. Spec Publ 43:97–113

Barbin V et al (1991) Cathodoluminescence of recent biogenic carbonates: an enviromental and onto genetic fingerprint. Geol Mag 128:19–26

Bartley JK, Kah LC (2004) Marine carbon reservoir, C_{org}–C_{carb} coupling, and the evolution of the proterozoic carbon cycle. Geology 32:129–132

Bruland KW, Middag R, Lohan MC (2014) Controls of trace metals in seawater A2—Holland, Heinrich D. In: Turekian KK (ed) Treatise on geochemistry, 2nd edn. Elsevier, Oxford, pp 19–51

Budd DA, Hammes U, Ward WB (2000) Cathodoluminescence in calcite cements: new insights on Pb and Zn sensitizing, Mn activation, and Fe quenching at low trace-element concentrations. J Sediment Res 70(1):217–226

Cai P et al (2014) ^{224}Ra:^{228}Th disequilibrium in coastal sediments: implications for solute transfer across the sediment–water interface. Geochimica et Cosmochimica Acta 125 (supplement C) :68–84

Cai P et al (2015) Using ^{224}Ra/^{228}Th disequilibrium to quantify benthic fluxes of dissolved inorganic carbon and nutrients into the Pearl River Estuary. Geochimica et Cosmochimica Acta 170 (supplement C) :188–203

Canfield DE, Thamdrup B (2009) Towards a consistent classification scheme for geochemical environments, or, why we wish the term 'suboxic' would go away. Geobiology 7:385–392

Canfield DE, Thamdrup B, Hansen JW (1993) The anaerobic degradation of organic matter in Danish coastal sediments: iron reduction, manganese reduction, and sulfate reduction. Geochim Cosmochim Acta 57:3867–3883

Chang J et al (2017) High resolution bio- and chemostratigraphic framework at the Frasnian-Famennian boundary: implications for regional stratigraphic correlation between different sedimentary facies in South China. Palaeogeogr, Palaeoclimatol, Palaeoecol. https://doi.org/10.1016/j.palaeo.2017.05.019

Chen D et al (2001a) Long-distance correlation between tectonic-controlled, isolated carbonate platforms by cyclostratigraphy and sequence stratigraphy in the Devonian of South China. Sedimentology 48(1):57–78

Chen D et al (2001b) Carbonate sedimentation in a starved pull-apart basin, Middle to Late Devonian, southern Guilin, South China. Basin Res 13(2):141–167

Chen D, Qing H, Yan X et al (2006) Hydrothermal venting and basin evolution (Devonian, South China): Constraints from rare earth element geochemistry of chert. Sediment Geol 183(3–4):203–216

Chen J et al (2018) Strontium and carbon isotopic evidence for decoupling of pCO_2 from continental weathering at the apex of the late Paleozoic glaciation. Geology 46:395–398

Clarkson MO et al (2014) Assessing the utility of Fe/Al and Fe-speciation to record water column redox conditions in carbonate-rich sediments. Chem Geol 382(11):111–122

Dupraz C et al (2009) Processes of carbonate precipitation in modern microbial mats. Earth Sci Rev 96(3):141–162

Edmonds J (1992) Himalayan tectonics, weathering processes, and the strontium isotope record in marine limestones. Science 258:1594

Emerson S, Hedges J, Heinrich DH, Karl KT (2003) Sediment Diagenesis and benthic flux, treatise on geochemistry. Pergamon, Oxford, pp 293–319

falFrerichs WE (1971) Evolution of planktonic foraminifera and paleotemperatures. J Paleontol 45(6):963–968

Fike DA, Bradley AS, Rose CV (2015) Rethinking the ancient sulfur cycle. Annu Rev Earth Planet Sci 43(1):593–622

Frimmel HE (2009) Trace element distribution in Neoproterozoic carbonates as palaeoenvironmental indicator. Chem Geol 258(3–4):338–353

Gallagher KL, Dupraz C, Visscher PT (2014) Two opposing effects of sulfate reduction on carbonate precipitation in normal marine, hypersaline, and alkaline environments: comment. Geology 42:e313–e314

Gill BC, Lyons TW, Frank TD (2008) Behavior of carbonate-associated sulfate during meteoric diagenesis and implications for the sulfur isotope paleoproxy. Geochim Cosmochim Acta 72(19):4699–4711

Gilleaudeau GJ, Kah LC (2013) Carbon isotope records in a Mesoproterozoic epicratonic sea: Carbon cycling in a low-oxygen world. Precambrian Res 228:85–101

Gupta BKS (1999) Systematics of modern foraminifera. In: Gupta BKS (ed) Modern foraminifera. Kluwer Academic Publishers, Dordrecht, pp 7–36

Halverson GP, Hoffman PF, Schrag DP, Maloof AC, Rice AHN (2005) Toward a Neoproterozoic composite carbon-isotope record. Geol Soc Am Bull 117:1181–1207

Hardie LA (1996) Secular variation in seawater chemistry: an explanation for the coupled secular variation in the mineralogies of marine limestones and potash evaporites over the past 600 m.y. Geology 24(3):279–283

Higgins JA, Schrag DP (2012) Records of Neogene seawater chemistry and diagenesis in deep-sea carbonate sediments and pore fluids. Earth Planet Sci Lett 357–358:386–396

Ji Q et al (1989) The Dapoushang section—an excellent section for the Devonian–Carboniferous boundary stratotype in China. Science Press, Beijing, pp 1–165

Jacobsen SB, Kaufman AJ (1999) The Sr, C and O isotopic evolution of Neoproterozoic seawater. Chem Geol 161:37–57

James NP, Choquette PW (1983) Diagenesis 6 limestones—the sea floor diagenetic environment. Geosci Can 10(4):162–179

Jiang G, Kaufman AJ, Christie-Blick N, Zhang S, Wu H (2007) Carbon isotope variability across the Ediacaran Yangtze platform in South China: implications for a large surface-to-deep ocean δ^{13}C gradient. Earth Planet Sci Lett 261(1–2):303–320

John SG, Mendez J, Moffett J, Adkins J (2012) The flux of iron and iron isotopes from San Pedro Basin sediments. Geochimica et Cosmochimica Acta 93(Supplement C):14–29

Jones CE, Jenkyns HC (2001) Seawater strontium isotopes, oceanic anoxic events, and seafloor hydrothermal activity in the Jurassic and cretaceous. Am J Sci 301(2):112–149

Kah LC, Lyons TW, Frank TD (2004) Low marine sulphate and protracted oxygenation of the Proterozoic biosphere. Nature 431:834–838

Kah LC, Bartley JK, Teal DA (2012) Chemostratigraphy of the Late Mesoproterozoic Atar Group, Taoudeni Basin, Mauritania: muted isotopic variability, facies correlation, and global isotopic trends. Precambrian Res 200–203:82–103

Kampschulte A, Strauss H (2004) The sulfur isotopic evolution of Phanerozoic seawater based on the analysis of structurally substituted sulfate in carbonates. Chem Geol 204:255–286

Kampschulte A, Bruckschen P, Strauss H (2001) The sulphur isotopic composition of trace sulphates in Carboniferous brachiopods: implications for coeval seawater, correlation with other geochemical cycles and isotope stratigraphy. Chem Geol 205:149–173

Kaufman AJ, Knoll AH (1995) Neoproterozoic variations in the C-isotope composition of sea water: stratigraphic and biogeochemical implications. Precambr Res 73(3–4):27–49

Kaufman AJ, Jacobsen SB, Knoll AH (1993) The Vendian record of Sr and C isotopic variations in seawater: implications for tectonics and paleoclimate. Earth Planet Sci Lett 120:409–430

Kaźmierczak J, Coleman ML, Gruszczyński M, Kempe S (1996) Cyanobacterial key to the genesis of micritic and peloidal limestones in ancient seas. Acta Palaeontol Pol 41:319–338

Knauth LP, Kennedy MJ (2009) The late Precambrian greening of the Earth. Nature 460(7256):728–732

Knoll AH, Hayes JM, Kaufman AJ, Swett K, Lambert IB (1986) Secular variation in carbon isotope ratios from Upper Proterozoic successions of Svalbard and east Greenland. Nature 321:832–838

Kump LR, Arthur MA (1999) Interpreting carbon-isotope excursions: carbonates and organic matter. Chem Geol 161:181–198

Lang X et al (2016) Ocean oxidation during the deposition of basal Ediacaran Doushantuo cap carbonates in the Yangtze Platform, South China. Precambr Res 281:253–268

Libes S (2009) Introduction to marine biogeochemistry. Elsevier Inc, Amsterdam

Lyons TW, Severmann S (2006) A critical look at iron paleoredox proxies: new insights from modern euxinic marine basins. Geochimica et Cosmochimica Acta 70(23):5698–5722

Ma H et al (2017) Heterogeneous Mg isotopic composition of the early Carboniferous limestone: implications for carbonate as a seawater archive. Acta Geochimica. https://doi.org/10.1007/s11631-017-0179-x

Machel H-G (1985) Cathodoluminescence in calcite and dolomite and its chemical interpretation. Geosci Can 12:139–147

Mackenzie FT, Morse JW (1992) Sedimentary carbonates through Phanerozoic time. Geochim Cosmochim Acta 56(8):3281–3295

Mackenzie FT, Lerman A, Andersson AJ (2004) Past and present of sediment and carbon biogeochemical cycling models. Biogeosciences 1(1):11–32

Mazzullo SJ (1992) Geochemical and neomorphic alteration of dolomite: a review. Carbonates & Evaporites 7(1):21

Morse JW, Bender ML (1990) Partition coefficients in calcite: examination of factors influencing the validity of experimental results and their application to natural systems. Chem Geol 82:265–277

Munnecke A, Samtleben C (1996) The formation of micritic limestones and the development of limestone-marl alternations in the Silurian of Gotland, Sweden. Facies 34(1):159–176

Myers CR, Nealson KH (1988) Bacterial manganese reduction and growth with manganese oxide as the sole electron acceptor. Science 240:1319

Nealson KH, Myers CR (1990) Iron reduction by bacteria: a potential role in the genesis of banded iron formations. Am J Sci 290:A35

Nie T et al (2016) Age and distribution of the Late Devonian brachiopod genus Dzieduszyckia Siemiradzki, 1909 in southern China. Palaeoworld 25(4):600–615

Nothdurft LD, Webb GE, Kamber BS (2004) Rare earth element geochemistry of Late Devonian reefal carbonates, Canning Basin, Western Australia: confirmation of a seawater REE proxy in ancient limestones. Geochim Cosmochim Acta 68(2):263–283

Pelechaty SM, Kaufman AJ, Grotzinger JP (1996) Evaluation of delta ^{13}C chemostratigraphy for intrabasinal correlation; Vendian strata of Northeast Siberia. Geol Soc Am Bull 108(8):992–1003

Pierson BJ (1981) The control of cathodoluminescence in dolomite by iron and manganese. Sedimentology 28(5):601–610

Pingitore NE Jr, Meitzner G, Love KM (1995) Identification of sulfate in natural carbonates by x-ray absorption spectroscopy. Geochim Cosmochim Acta 59:2477–2483

Pogge von Strandmann PAE, Forshaw J, Schmidt DN (2014) Modern and Cenozoic records of seawater magnesium from foraminiferal Mg isotopes. Biogeosciences 11:5155–5168

Poulton SW, Raiswell R (2002) The low-temperature geochemical cycle of iron: from continental fluxes tomarine sediment deposition. Am J Sci 302(9):774–805

Poulton SW, Canfield DE (2005) Development of a sequential extraction procedure for iron: implications for iron partitioning in continentally derived particulates. Chem Geol 214:209–221

Poulton SW, Canfield DE (2011) Ferruginous conditions: a dominant feature of the ocean through Earth's history. Elements 7(2):107–112

Raiswell R, Canfield DE (1998) Sources of iron for pyrite formation in marine sediments. Am J Sci 298(3):219–245

Richter F, Rowley DB, DePaolo DJ (1992) Sr isotope evolution of seawater: the role of tectonics. Earth Planet Sci Lett 109:11–23

Riding R (1991) Classification of microbial carbonates. In: Riding R (ed) Calcareous algae and stromatolites. Springer, Berlin, pp 21–87

Rudnick RL, Gao S (2003) Composition of the continental crust. In: Rudnick RL (ed) The crust. Treatise on geochemistry. Elsevier-Pergamon, Oxford, pp 1–64

Ruppel SC et al (1996) High-resolution $^{87}Sr/^{86}Sr$ chemostratigraphy of the Silurian: implications for event correlation and strontium flux. Geology 24:831–834

Saltzman MR et al (2014) Calibration of a conodont apatite-based Ordovician $^{87}Sr/^{86}Sr$ curve to biostratigraphy and geochronology: implications for stratigraphic resolution. Geol Soc Am Bull 126(11–12):1551–1568. https://doi.org/10.1130/b31038.1

Sepkoski JJ Jr, Miller AI (1985) Evolutionary faunas and the distribution of Paleozoic benthic communities. In: Valentine JW (ed) Phanerozoic diversity patterns: profiles in macroevolution. Princeton University Press, Princeton, pp 153–190

Severmann S, McManus J, Berelson WM, Hammond DE (2010) The continental shelf benthic iron flux and its isotope composition. Geochim Cosmochim Acta 74(14):3984–4004

Shaw HF, Wasserburg GJ (1985) Sm-Nd in marine carbonates and phosphates; implications for Nd isotopes in seawater and crustal ages. Geochim Cosmochim Acta 49(2):503–518

Shen B et al (2011) Carbon, sulfur, and oxygen isotope evidence for a strong depth gradient and oceanic oxidation after the Ediacaran Hankalchough glaciation. Geochim Cosmochim Acta 75(5):1357–1373

Sperling EA et al (2015) Statistical analysis of iron geochemical data suggests limited late Proterozoic oxygenation. Nature 523(7561):451–454

Stanley SM, Hardie LA (1998) Secular oscillations in the carbonate mineralogy of reef-building and sediment-producing organisms driven by tectonically forced shifts in seawater chemistry. Palaeogeogr Palaeoclimatol Palaeoecol 144(1–2):3–19

Stanley SM, Hardie LA (1999) Hypercalcification: Paleontology links plate tectonics and geochemistry to sedimentology. Gsa Today 9(2):1–7

Tucker ME, Wright VP (1990) Carbonate sedimentology. Blackwell, Oxford, p 482

Vachard D, Pille L, Gaillot J (2010) Palaeozoic Foraminifera: systematics, palaeoecology and responses to global changes. Rev Micropaléontol 5:209–254

Verbruggen H, Clerck OD, Schils T, Kooistra WHCF, Coppejans E (2005) Evolution and phylogeography of Halimeda section Halimeda (Bryopsidales, Chlorophyta). Mol Phylogenet Evol 37(3):789–803

Webb GE, Kamber BS (2000) Rare earth elements in Holocene reefal microbialites: a new shallow seawater proxy. Geochim Cosmochim Acta 64(9):1557–1565

Wefer G (1980) Carbonate production by algae Halimeda, Penicillus and Padina. Nature 285:323

Wehrmann LM et al (2014) Iron and manganese speciation and cycling in glacially influenced high-latitude fjord sediments (West Spitsbergen, Svalbard): evidence for a benthic recycling-transport mechanism. Geochim Cosmochim Acta 141(supplement C):628–655

Zeng Y, Liu T (1999) Characteristics of the Devonian Xialei manganese deposit, Guangxi Zhuang Autonomous Region, China. Ore Geol Rev 15:153–163

Zhao Y-Y, Zheng Y-F, Chen F (2009) Trace element and strontium isotope constraints on sedimentary environment of Ediacaran carbonates in southern Anhui, South China. Chem Geol 265(3–4):345–362

Zhu M, Zhang J, Yang A (2007) Integrated Ediacaran (Sinian) chronostratigraphy of South China. Palaeogeogr Palaeoclimatol Palaeoecol 254(1–2):7–61

Zhu M et al (2013) Carbon isotope chemostratigraphy and sedimentary facies evolution of the Ediacaran Doushantuo Formation in western Hubei, South China. Precambr Res 225:7–28